CONFERENCE PRE-PRINT

THEORY-BASED INTEGRATED MODELLING OF TUNGSTEN TRANSPORT

Validation in present-day tokamaks and predictions for ITER

D. FAJARDO
Max Planck Institute for Plasma Physics
Garching, Germany
Email: daniel.fajardo@ipp.mpg.de

C. ANGIONI, E. FABLE, G. TARDINI
Max Planck Institute for Plasma Physics
Garching, Germany

C. GIROUD, M. PORADZINSKI
United Kingdom Atomic Energy Authority
Abingdon, United Kingdom

S. H. KIM, F. KOECHL, A. LOARTE
ITER Organization
St. Paul lez Durance, France

Abstract

Using state-of-the-art theoretical transport models in an integrated tokamak modelling workflow, it is demonstrated that the physics of tungsten (W) transport in the core of a fusion reactor is in a markedly different regime as compared to present-day experiments, which has profound implications for the operation of the now fully-W-walled ITER fusion device. The workflow, based on the ASTRA transport code and the TGLF-SAT2 quasi-linear turbulent transport and FACIT neoclassical impurity transport models, has been validated against experimental data in ASDEX Upgrade and JET-ILW. In particular, with this modelling approach, by condensing the recently developed theoretical knowledge on heavy impurity transport, for the first time quantitative predictions of the power requirements to avoid central W accumulation in present experiments have been achieved. This provides confidence on the physics understanding of high-Z impurity transport for extrapolation to future reactors. In ITER, the challenges introduced by W arise from global radiation losses that can hinder operation in H-mode, instead of local central accumulation as in present-day devices. The analysis reveals the interplay between the W content in the plasma, the applied auxiliary heating power, and the quality of the energy confinement, allowing the determination of the domain over which stable operation in H-mode at 15 MA can be expected and the ITER fusion performance targets can be achieved. Furthermore, the access and sustainment of the H-mode at lower current as well as the plasma survival during the current ramp-up are analyzed at increasing W concentrations.

1. INTRODUCTION

Predicting the behavior of impurities and their compatibility with fusion performance has become critical as magnetic fusion devices approach reactor-relevant operation. Practically all next-generation fusion devices, including ITER [1], plan to use fully metallic plasma facing components, and integrating high-Z materials like tungsten (W) with core plasma performance is challenging because they radiate away plasma energy very efficiently [2]. At the same time, the extreme heat fluxes incident on the divertor targets will likely require high impurity seeding for safe power exhaust at the edge, with high radiative power fractions.

We present an integrated modelling workflow that self-consistently describes impurity transport and the feedback effects of impurities on the main plasma via radiation and fuel dilution. It is based entirely on theoretical

transport models, and it is described in section 2. A comprehensive validation effort is performed against experimental data from ASDEX Upgrade (AUG) and JET-ILW, including full-radius simulations of seeded L-modes and modelling of W accumulation control with central wave heating in beam-heated H-modes, which is presented in section 3. This validation provides confidence on the physics understanding of impurity transport for extrapolation to future reactors. Section 4 is then dedicated to the analysis of a variety of ITER plasmas, focusing on the interplay between W transport, auxiliary heating and fusion performance. Finally, section 5 summarizes the work and discusses the implications of impurity transport in reactors.

2. THEORY-BASED MODELLING WORKFLOW

The modelling workflow employed to study these plasmas is largely the one described in [3]. The modules for transport, heat and particle sources, and equilibrium are integrated in ASTRA [4]. Transport coefficients are obtained with theory-based models: the TGLF-SAT2 [5] quasilinear model is employed to compute the turbulent transport coefficients, while FACIT [6] is used to obtain neoclassical impurity transport coefficients. For all simulations, the electron and ion temperatures (T_e, T_i), the electron density (n_e), the current density (j), W as a heavy impurity and a lighter impurity (B, Ne or Ar) are evolved. The toroidal rotation (v_φ) is prescribed to measured profiles or, for ITER modelling, to previous predictions in the literature (15 MA H-modes) or to zero (L-modes). In full-radius simulations, the particle content is assigned in feedback. The STRAHL code [7] is used to calculate the impurity distribution and radiation. By condensing the recently developed theoretical knowledge on local neoclassical and quasi-linear turbulent high-Z impurity transport, in particular effects connected to poloidal asymmetries in the impurity densities, the workflow is able to capture physics leading to impurity profiles ranging from very hollow, to flat, to very peaked in different tokamak plasma scenarios.

3. INTEGRATED MODELLING VALIDATED AGAINST ASDEX UPGRADE AND JET EXPERIMENTS

3.1. Full-radius modelling of seeded L-mode plasmas

We begin the validation effort on an AUG radiative L-mode with high heating power (> 7 MW), kept just below the L-H threshold by feedback control on the power crossing the separatrix using argon (Ar) seeding as actuator. AUG #37041 features high confinement ($H_{98} \approx 0.95$) and no edge localized modes (ELMs) with an X-point radiator (XPR) [8]. It is an appealing application due to the high impurity content and radiated power, the presence of multiple species (intrinsic B and W, seeded Ar) and the high confinement with no ELM activity. The coupled evolution of multiple transport channels, including the three impurities, leads to good agreement between the simulated and measured profiles [3], as it is shown in Fig. 1, the high radiated power fraction and the H-mode-like confinement. A simple XPR model has been applied to account for highly edge-localized radiation [3]. The stabilizing effect of impurities on core turbulence has been analyzed, by performing an additional simulation without impurities, finding that without Ar confinement decreases by $\sim 33\%$ [3].

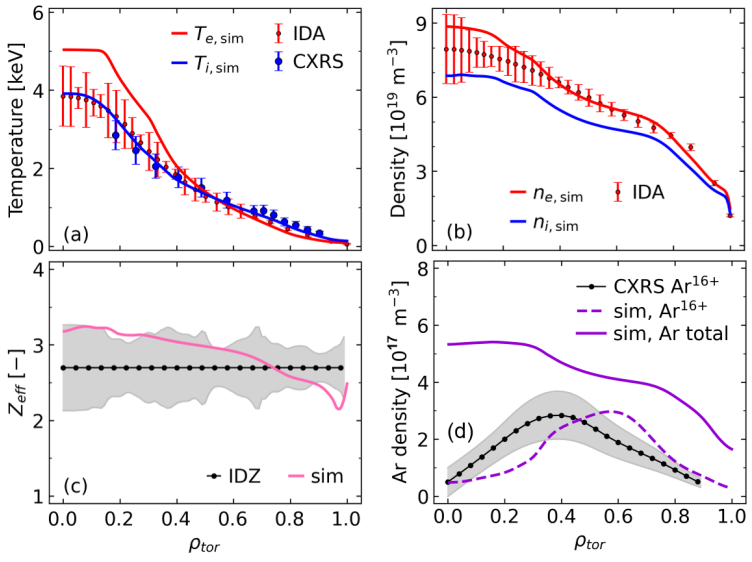

FIG. 1. Full-radius simulation against measurements of AUG #37041. (a) Electron and ion temperatures, (b) electron and D densities, (c) effective charge and (d) argon density. Adapted from figure 6 of [3] CC BY 4.0.

Furthermore, we simulate three JET-ILW plasmas with high heating power (> 30 MW) and neon seeding, at approximately constant discharge parameters except for a scan of Ne gas puff. They are deuterium (D) plasmas with high current $I_p = 3.2$ MA at $B_t = 3.45$ T ($q_{95} \approx 3.3$), and feature a mild rotation. Despite the high heating power, a strong pedestal does not build up [9], which allows us to apply TGLF up to the separatrix.

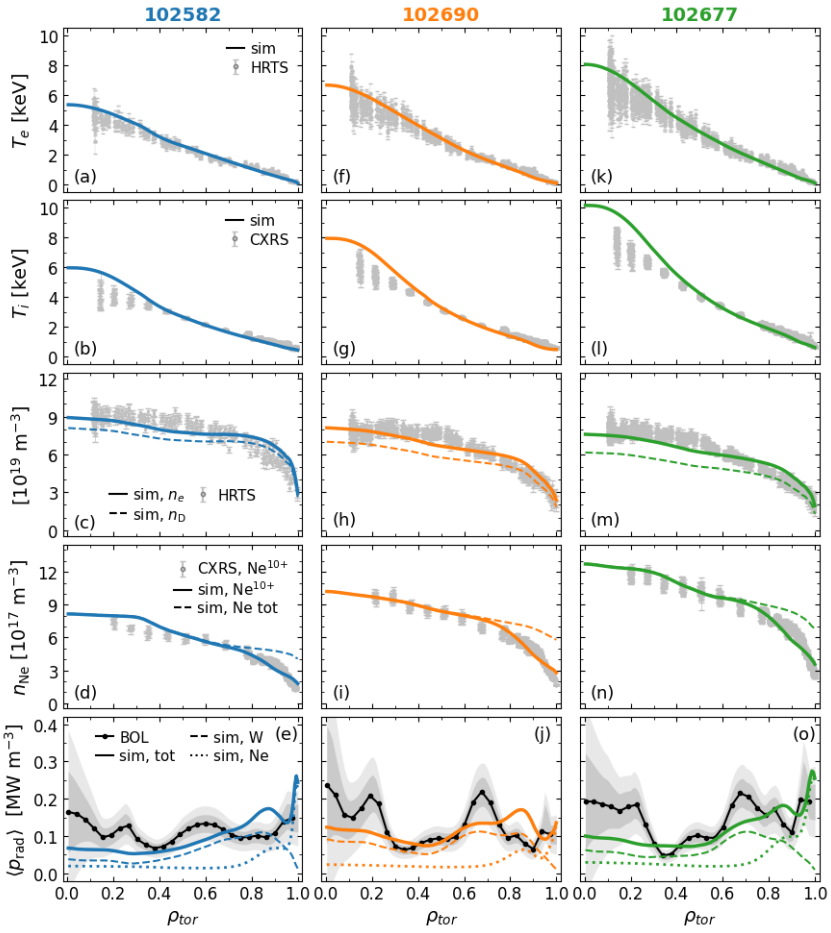

FIG. 2. Simulated profiles against measurements for the JET-ILW pulses with a neon seeding scan. (a) Electron and (b) ion temperatures, (c) electron density (D density in dashed lines), (d) Ne^{10+} density, (e) radiated power density (components by W and Ne in dashed and dotted lines), for the 'low' seeding case 102582. (f–j) Same as (a–e) but for the 'intermediate' seeding case 102690. (k–o) Same as (a–e) but for the 'high' seeding case 102677.

The T_e and T_i are overall closely reproduced in the three pulses, as shown in Fig. 2, with only a slight over-estimation of the central T_i. As the Ne content increases, the measured temperatures increase which is captured by the modelling. The electron densities are relatively flat in both predictions and measurements, and there is a decrease in density as the Ne seeding increases. Parallel simulations removing the Ne show a decrease in the stored energy $W_{\rm th}$ of 10–30% with respect to the simulations with Ne, due entirely to the increase in the temperatures. This increase of confinement with Ne is not dramatic, but including Ne in the simulations is important to reproduce the measured $W_{\rm th}$. The predicted Ne^{10+} density matches the measurement quite well, with a mildly peaked core and a steeper edge gradient. Finally, the radiated power density obtained from flux surface averages of the 2D tomographic inversions of bolometry is compared to the simulated radiation, which is mostly due to W and Ne and it is generally flat. Ne radiates mostly at the periphery, $\rho_{\rm tor} > 0.85$, whereas W does not radiate much at the edge but rather farther in, with a radiation peak around the location of $T_e \approx 1.5$ keV.

3.2. Control of tungsten accumulation with central wave heating in AUG

In present-day tokamaks, routine operation with neutral beam injection (NBI) also requires central wave heating to avoid core W accumulation and a subsequent local radiative collapse of the plasma center. The use of central electron and ion cyclotron resonance heating (ECRH, ICRH) to control high-Z impurity accumulation is a well-established technique across multiple fusion devices, whose physics basis is a simultaneous enhancement of the turbulent impurity diffusivity and a reduction of the neoclassical pinch, both leading to flatter impurity

profiles. The ability to reproduce these effects is an important validation for an integrated modelling workflow that predicts impurity transport and radiation self-consistently.

The workflow described in section 2 recovers essential physics of W transport in the presence of central wave heating, quantitatively reproducing experimental observations of AUG H-modes with constant NBI and power steps in ECRH [10]. Fig. 3 shows an example of the good agreement between simulation and measurements when the plasma temperature and density profiles, the W density and the radiation are self-consistently evolved.

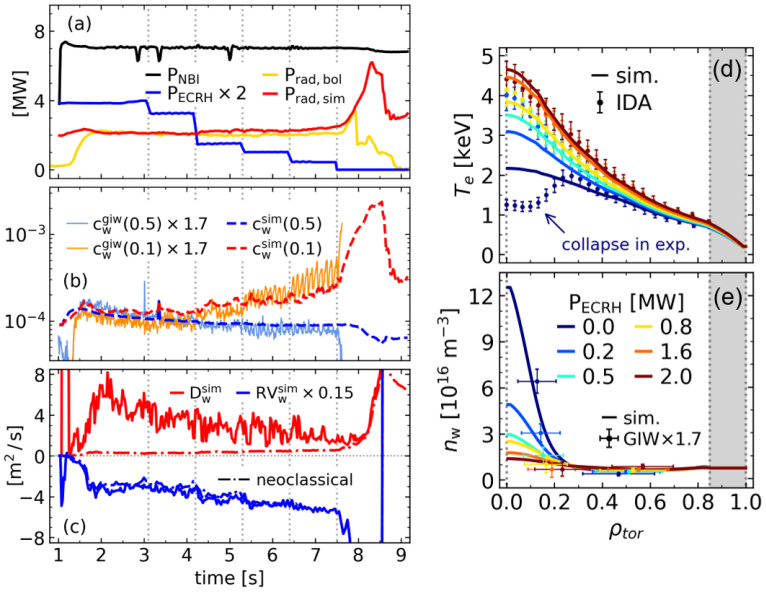

FIG. 3. Dynamical integrated modelling of AUG #32408. Time traces of (a) heating and radiated powers, (b) simulated and measured on- and off-axis W concentrations, (c) central W diffusivity and convection (total, solid) with their neoclassical components (dashed). Simulated and measured profiles of (d) the electron temperature and (e) the W density as a function of the ECRH power. Adapted from figures 1 and 2 of [10] CC BY 4.0.

The dynamical evolution of the entire flat-top of AUG #32408 captures the flattening of W when central ECRH is applied, as well as conditions of runaway accumulation once the ECRH is removed [10]. There is quantitative agreement with the measured time trajectories of the radiated power and W concentrations, as well as the measured plasma profiles at the different phases of the discharge [10]. Furthermore, the physics of an enhanced turbulent W diffusivity and reduced neoclassical pinch with higher ECRH is captured by the theory-based transport models, paving the path for quantitative predictions of the required levels of central wave heating for W accumulation control in future devices [10].

4. PREDICTIVE MODELLING OF ITER: INTERPLAY BETWEEN IMPURITY TRANSPORT, PLASMA HEATING AND FUSION PERFORMANCE

Having validated the theory-based workflow on AUG and JET, the attention is shifted to integrated modelling predictions of a variety of ITER plasmas. Multiple simulations span the range from the 15 MA baseline H-mode scenario in DT, to lower current electron-heated L-modes in D (5 & 7.5 MA), to dynamical modelling of the current ramp-up. Particular emphasis is placed on the transport and effects of tungsten, following the new ITER baseline and its replacement of Be for W as a first wall material [1].

4.1. ITER 15 MA baseline scenario

In the core of a reactor like ITER, the much higher temperatures lead to a much lower collisionality compared to the core of present day devices. This, in addition to the lower expected toroidal rotation and lack of a central particle source, leads to a strong reduction of neoclassical high-Z impurity transport. The core W convection is dominated by turbulence, in contrast to the mostly neoclassical W convection which is responsible for problematic central W peaking in present-day tokamaks. This is shown in Fig. 4 for a scan in ECRH power in core conditions for an AUG H-mode with NBI and the ITER 15 MA baseline H-mode.

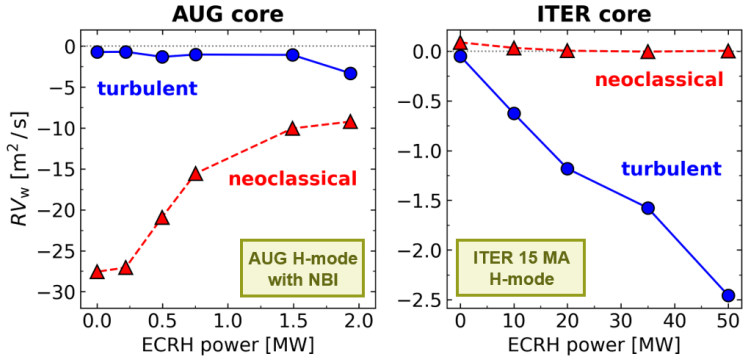

FIG. 4. Core tungsten neoclassical and turbulent convection as a function of central ECRH power for an AUG NBI H-mode (left) and the ITER 15 MA baseline scenario (right).

Turbulent transport does not produce any mechanism of strong inward convection of high-Z impurities [11], yielding relatively flat core W density profiles regardless of the level of ECRH in ITER 15 MA plasmas [10], as shown on the right of Fig. 5. In comparison to the AUG W densities in figure 3(e), there are no conditions of central W peaking in the ITER core, even without ECRH, because the neoclassical convection is sub-dominant [10]. Across the pedestal the collisionality increases and there is considerable neoclassical temperature screening for W. The corresponding simulated main plasma profiles are shown on the left of Fig. 5.

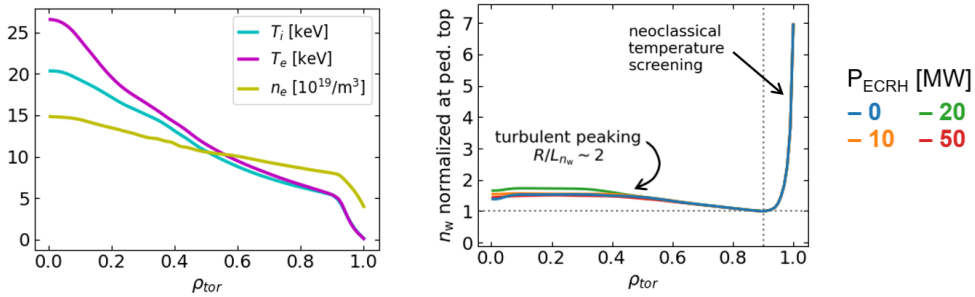

FIG. 5. Simulated T_i, T_e and n_e for the ITER 15 MA baseline scenario with 30 MW of NBI and 20 MW of ECRH and a pedestal top pressure of 130 kPa as boundary condition (left). W density profiles, normalized to the pedestal top, for different values of the ECRH power (right). Right figure adapted from figure 5 of [10] CC BY 4.0.

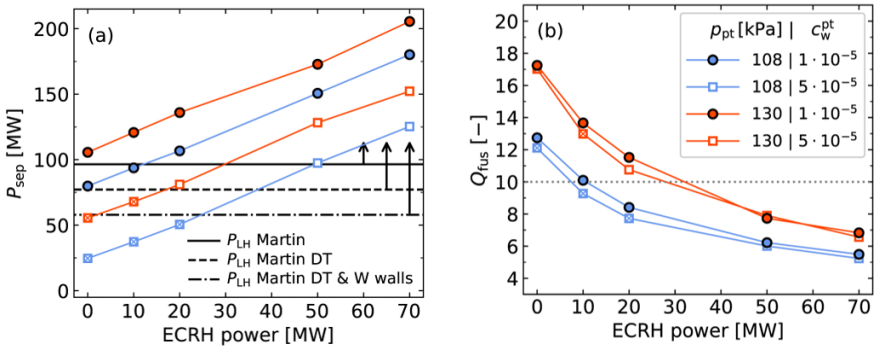

FIG. 6. (a) Power crossing the separatrix and (b) fusion power multiplication factor, as a function of ECRH. Comparison of confinement assumptions with pedestal top pressure 20% below (blue, $H_{98} \approx 0.85$) and at the peeling-ballooning limit (red, $H_{98} \approx 1.05$), as well as with intermediate (full symbols) and high (open) W concentrations. Additional 30 MW of NBI are applied. The symbols with crosses indicate conditions that would go below the Martin L-H power threshold scaling [12] with isotope effects. Adapted from figure 1 of [13] CC BY 4.0.

A radiative collapse by a negative power balance locally in the inner core is therefore not expected thanks to the lack of W accumulation. The limiting effect as the edge W concentration increases is produced by the global radiation losses which would not allow the power crossing the separatrix to sustain the H-mode regime [10]. Auxiliary heating can be increased to compensate for impurity radiation, but this comes at a cost on the fusion performance in $Q_{\rm fus} = P_{\rm fus}/P_{\rm aux}$ (recent IMEP results found little sensitivity of the pedestal pressure to the

ECRH power in ITER [14]). This is investigated in Fig. 6. 20 simulations are carried out at two different pedestal top pressures (130 and 108 kPa), for a low and a high pedestal top W concentration (10^{-5} and 5×10^{-5}), and a scan in ECRH powers $\{0, 10, 20, 50, 70\}$ MW. The higher confinement (peeling-ballooning limited pedestal, red) leads to a stronger alpha heating that provides a larger margin for H-mode sustainment and a higher tolerable W concentration with respect to the lower pedestal (blue, mimicking ELM-free operation) [13]. The TGLF-SAT2 predictions with the higher pedestal top pressure comfortably satisfy the ITER targets of $Q_{\rm fus} = 10$ and $P_{\rm fus} = 500$ MW. $Q_{\rm fus} > 10$ target can be accessed by reducing the auxiliary heating, provided that the W concentration is not too high ($\leq 5 \times 10^{-5}$) [13].

4.2. ITER L-modes with ECRH at lower current and field

Full-radius modelling in L-mode is performed at lower currents in electron-heated D plasmas to assess the maximum W concentrations that allow access to H-mode operation, scanning the separatrix W concentration ($c_{\rm w}^{\rm sep}$) in multiple simulations for three scenarios: 5.0 MA with 20 MW of ECRH, 5.0 MA with 40 MW and 7.5 MA with 40 MW [13]. Fig. 7 summarizes the results of the simulations for the three scenarios and for the different $c_{\rm w}^{\rm sep} \in \{0 - 5 \times 10^{-4}\}$. The T_e profiles are quite similar at the same heating of 40 MW between different currents, and lower at 20 MW of ECRH, whereas the T_i profiles is somewhat more peaked at higher current. The n_e magnitude is higher at higher current, because the Greenwald fraction is kept constant, but it is also more peaked. Therefore an increase of global confinement is predicted at higher current and density [13]. The different $c_{\rm w}^{\rm sep}$ do not dramatically influence the shape of the T_e, T_i and n_e profiles [13].

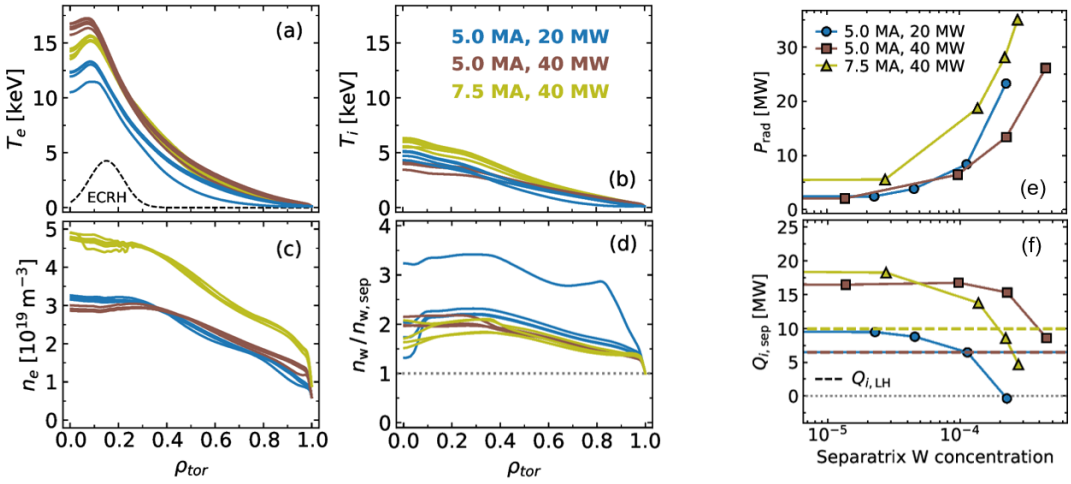

FIG. 7. (left and center) Simulated ITER L-mode profiles at different currents and ECRH powers (in different colors). The different lines of a single color represent the five simulations at increasing W concentration. (a) Electron and (b) ion temperatures, (c) electron and (d) W density. (right) Scan in the separatrix W concentration. (e) Radiated power and (f) ion heat flux reaching the separatrix, with Schmidmayr L-H scaling [15] in dashed lines. Adapted from figures 4 and 5 of [13] CC BY 4.0.

The W densities are still rather flat in the core, similarly to the ITER H-modes, but contrary to the ITER H-modes, the edge W density is not hollow, due to a lack of strong neoclassical temperature screening [13]. Access to H-mode is assessed by calculating the ion heat flux Q_i reaching the separatrix as a function of the radiated power caused by the increasing W content. Comparing this Q_i to the Schmidtmayr L-H transition scaling [15] allows us to identify the maximum tolerable W concentrations to access H-mode at a given current and ECRH power. These results are consistent with the ones of [16], where the W densities were prescribed.

4.3. Current ramp-up

The current ramp-up is a critical phase in terms of impurity transport. The new full-W first wall of ITER brings particular interest to the limiter phase. We perform full-radius dynamical simulations of the ITER I_p ramp-up, including W transport and radiation at three different levels of W sources. This allows us to identify maximum tolerable W concentrations to avoid a radiative collapse of the plasma [13]. Fig. 8 summarizes the results. On the left, the last closed flux surface is shown from the limiter to the diverted phase across 65 s of I_p ramp going from 2 to 15 MA. The corresponding relevant time traces of the simulation are shown on the center and right. At the maximum possible W concentration of 2.5×10^{-4} during the limiter phase, the combination of ECRH and

Ohmic heating just marginally compensate radiated power losses [13]. Even though the trajectories of the central temperatures and line-averaged density are not noticeably modified by the level of W content, the loop voltage and internal inductance increase in the case that barely survives the radiative collapse compared to the cases at lower or no W, leading to a higher flux consumption by around 20% [13]. This type of modelling also allows the optimization of the time trajectory of ECRH power to tolerate higher W content in critical ramp-up phases [13].

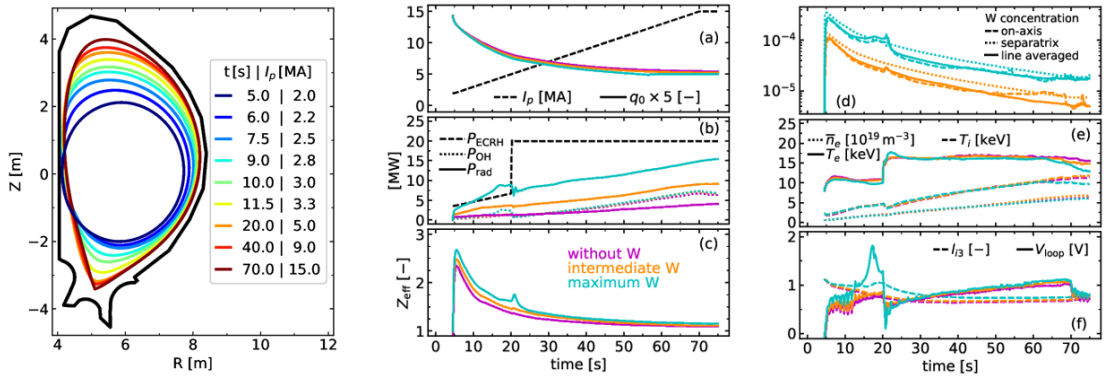

FIG. 8. (left) Evolution of the last closed flux surface during the ITER ramp-up simulations. (center and right) Time traces of the ramp-up simulations at increasing W sources (in different colors). (a) Plasma current (dashed) and safety factor on axis (solid, multiplied by 5). (b) ECRH (dashed), Ohmic (dotted) and radiated (solid) powers. (c) Line-averaged effective charge. (d) W concentration on axis (dashed), at the separatrix (dotted), and line-averaged (solid). (e) Line-averaged n_e (dotted), central T_e (solid) and central T_i (dashed). (e) Loop voltage (solid) and internal inductance (dashed). Adapted from figures 6 and 7 of [13] CC BY 4.0

.

5. SUMMARY AND CONCLUSIONS

An integrated modelling workflow that includes impurity transport and radiation has been presented. A notable feature of this workflow is that it is entirely based on theoretical transport models. The combination of TGLF-SAT2 and FACIT has been shown to capture important physics in the competition between neoclassical and turbulent high-Z impurity transport. The modelling workflow is able to quantitatively reproduce the experimental evolution of AUG H-mode plasmas as central wave heating is ramped down, going from conditions of flat W densities to a runaway W accumulation in the core and a subsequent radiative collapse of the plasma. Likewise, for a set of AUG and JET seeded discharges, the transport of both the seeded species and W as well as the stabilizing effect of impurities on turbulence have been analyzed and successfully validated against measurements of multiple transport channels. These validation efforts provide confidence on the application of the workflow to predict plasmas in future devices like ITER.

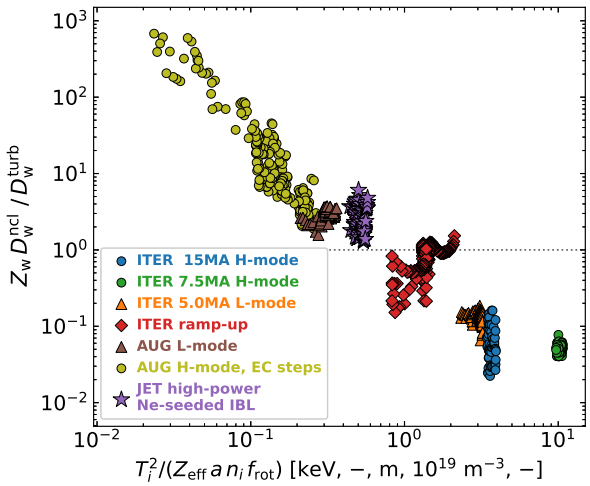

FIG. 9. Reduction of magnitude of core neoclassical W convection with respect to turbulent diffusion, going from plasma parameters in present-day devices to reactors. Adapted from figure 11 of [13] CC BY 4.0.

Approaching reactor core conditions of significantly higher temperatures, the decrease in collisionality and increase of the gyro-Bohm (gB) factor of turbulent transport implies that the magnitude of neoclassical transport is expected to decrease with respect to the magnitude of turbulent transport [17]. Consistently, this reduction of relative magnitudes of neoclassical to turbulent W transport, and the subsequent flat core W density profiles, have been obtained in ASTRA simulations of ITER plasmas using TGLF-SAT2 and FACIT theory-based transport models. This is shown in Fig. 9, where the change in transport regime for W can be ordered by a simple physical parameter (as explained in [13]).

The self-consistent evolution of the plasma and of the impurities allows us to determine the operational space of ITER in view of its full-W walls. Global radiative losses can hinder the access and sustainment of the H-mode and the survival of the plasma during the ramp-up phase. Wave heating can serve as an actuator to control the effects of W radiation, by allowing the plasma to tolerate a higher W concentration while remaining in H-mode, instead of by flattening the central W density, as in present-day devices. However, a higher auxiliary heating leads to a decrease of the fusion power multiplication factor $Q_{\rm fus}$, due to the limited increase of both the pedestal pressure [14] and the central temperatures with increasing power. With a peeling-ballooning limited pedestal, the models and assumptions of this work lead to a comfortable achievement of ITER's $Q_{\rm fus} = 10$ objective at 20 MW of ECRH + 30 MW of NBI, even with a fairly high W concentration in the plasma.

This work demonstrates new theory-based predictive capabilities which have been validated against experimental data and allow for an improved understanding of ITER plasmas.

ACKNOWLEDGEMENTS

This work has been carried out within the framework of the EUROfusion Consortium, funded by the European Union via the Euratom Research and Training Programme (Grant Agreement No 101052200-EUROfusion). Views and opinions expressed are however those of the authors only and do not necessarily reflect those of the European Union or the European Commission. Neither the European Union nor the European Commission can be held responsible for them.

REFERENCES

REFERENCES

[1] Loarte A. *et al* 2025 *Plasma Phys. Control. Fusion* **67** 065023

[2] Angioni C. 2025 *Nucl. Fusion* **65** 062001

[3] Fajardo D. *et al* 2024 *Nucl. Fusion* **64** 046021

[4] Fable E. *et al* 2013 *Plasma Phys. Control. Fusion* **55** 124028

[5] Staebler G. M. *et al* 2021 *Nucl. Fusion* **61** 116007

[6] Fajardo D. *et al* 2023 *Plasma Phys. Control. Fusion* **65** 035021

[7] Dux R. 2006 Tech. rep. IPP 10/30

[8] Fable E. *et al* 2021 *Nucl. Fusion* **62** 024001

[9] Giroud C. *et al*, *EX/C-2924* IAEA FEC 2025.

[10] Fajardo D. *et al* 2024 *Nucl. Fusion* **64** 104001

[11] Angioni C. 2021 *Plasma Phys. Control. Fusion* **63** 073001

[12] Martin Y. R. *et al* 2008 *J. Phys.: Conf. Ser.* **123** 012033

[13] Fajardo D. *et al* 2025 *Plasma Phys. Control. Fusion* **67** 015020

[14] Luda T. *et al* 2025 *Nucl. Fusion* **65** 072001

[15] Schmidtmayr M. *et al* 2018 *Nucl. Fusion* **58** 056003

[16] Angioni C. *et al* 2023 *Nucl. Fusion* **63** 126035

[17] Angioni C. *et al* 2017 *Nucl. Fusion* **57** 022009